Removal of phenol from wastewater using spiral-wound reverse osmosis process: model development based on experiment and simulation

Al-Obaidi M. A.[1, 2], Kara-Zaïtri C.[1] and Mujtaba I. M. [1, *]

[1] Chemical Engineering Division. School of Engineering, University of Bradford, West Yorkshire BD7 1DP, UK

[2] Middle Technical University, Iraq – Baghdad

***Corresponding author, Tel.: +44 0 1274 233645**

E-mail address: I.M.Mujtaba@bradford.ac.uk

Abstract

The removal of the ubiquitous phenol and phenolic compounds in industrial wastes is a critical environmental issue due to their harmful threats to wildlife and potential adverse human health effects. The removal of such compounds is therefore of significant importance in water treatment and reuse. In recent years, reverse osmosis (RO) has been successfully utilised in several industrial processes and wastewater treatment including phenol removal. In this paper, a new model based on a spiral-wound RO process is developed for the removal of phenol from wastewater. A simplified mathematical algorithm using an irreversible thermodynamic approach is developed. This results in a set of non-linear Differential and Algebraic Equations (DAEs), which are solved based on a number of optimised model parameters using a combined methodology of parameter estimation and experimental phenol-water data derived from the literature. The effects of several operational parameters on the performance (in terms of removal of phenol) of the process are explored using the model.

***Keywords*:** Wastewater treatment; Spiral-wound reverse osmosis; Distributed model;

Irreversible thermodynamic model; Phenol removal.

1. Introduction

The heavily industrial world we live in today continues to generate large volumes of wastewater containing industrial effluents, sewage and other harmful by-products, which are disposed into rivers and oceans. At the same time, the need for clean potable water continues to increase at a worrying rate due to increase in population and associated demand. The urgent need to treat and reuse water has never been greater in the modern world.

This paper focuses on developing efficient methods for treating wastewater by improving the reliability and efficiency of the underlying separation and filtration processes. The net result

of this work is the significant reduction of the probability of accidental release of these harmful compounds into the recycled water by implementing different water treatment approaches in many indirect potable water reuse schemes (Traves *et al.*, 2008).

Phenol and phenol compounds (aromatic compounds) represent a significant group of pollutants present in wastewater resulting from the manufacture of pesticides, herbicides, disinfectants, pharmaceuticals and dyes (Gami *et al.*, 2014). Also, the presence of trace amounts of these compounds has restricted the reuse of water in different industrial applications (Mangrulkar *et al.*, 2008). The successful treatment processes of phenol compounds removal from wastewater include catalytic wet air oxidation (CWAO), UV/H_2O_2 and RO. CWAO used trickle bed reactor using CUO, Zn, CO oxides as a heterogeneous catalyst and pure oxygen as oxidant of phenol (Mohammed *et al.*, 2016). However, the UV/H_2O_2 process requires a lot of energy but with a risk of increasing the carbon concentration of the reused water (Fujioka, 2014a). Among these technologies, RO is very promising, because of its ability to remove water/wastewater constituents such as phenol compounds (Schutte, 2003; Bódalo-Santoyo *et al.*, 2004; Alzahrani *et al.*, 2013). Additionally, the rapid growth of RO as a commercially attractive separation process in seawater desalination has paved the way for industrial effluents treatment as a promising technology for water recycling and reuse (Elhalwagi, 1992; Lee and Lueptow, 2001). Thus, seawater desalination and wastewater treatment are the core technologies for producing clean water (Wang *et al.*, 2016) and provided valuable opportunity to avoid the complete diminution of fresh water resources (Goh *et al.*, 2016). Specifically, the use of RO as a key treatment process in water reclamation applications has been confirmed to offer several advantages including; minimum thermal damage, high packing density as well as lower energy consumption (Fritzmann *et al.*, 2007).

Several RO theoretical transport models have been explored by various researchers to predict solute and solvent fluxes resulting in three types of models; the pore model (diffusion and convection-based), the nonporous model (diffusion–based) and the phenomenological model based on thermodynamic (Soltanieh and Gill, 1981). The solution-diffusion and the irreversible thermodynamic models are the most widely used to describe the performance of membrane separation systems. The validity of these models has been tested by Murthy and Gupta (1999) who confirmed that the Spiegler and Kedem model is more accurate for estimating the membrane performance. Having said this, Mujtaba (2012) showed that the solution-diffusion model is the simplest model and one that is widely used for describing the mechanism of transport in RO systems. Geraldes *et al.* (2005) have developed a one-

dimensional model for spiral-wound RO membranes based on the solution-diffusion model but neglected the diffusion flow in the feed side. Sagne *et al.* (2009) have considered an unsteady state one-dimensional model based on the solution-diffusion model for the rejection of dilute aqueous solution of five volatile organic compounds from brackish water. However, the model neglected the concentration polarisation impact. Oh *et al.* (2009) developed a one-dimensional model based on the solution-diffusion model to analyse the performance of a spiral-wound RO process. This assumes a constant mass transfer coefficient and a constant water flux. Kaghazchi *et al.* (2010) proposed a one-dimensional model based on the solution-diffusion model and the bulk flow rate is calculated as an average value of inlet and outlet feed flow rates.

In summary, sea and brackish water desalination have been extensively modelled as one-dimensional models with several assumptions (Senthilmurugan *et al.*, 2005). However, a limited number of published models describing spiral-wound RO process especially for wastewater treatment is available in the literature (Sundaramoorthy *et al.*, 2011a).

For example, Ahmad *et al.* (2007) developed a lumped model for unsteady state simulation based on the extended Spiegler and Kedem model. They then validated it with experimental data of pre-treated palm oil mill effluent as a feed using a pilot plant scale RO system. Verliefde *et al.* (2009) proposed a transport model based on the Spiegler and Kedem model for the rejection of organic solutes for nano-filtration membranes. While, Sundaramoorthy *et al.* (2011a, b) developed a one-dimensional model by assuming the validity of the solution-diffusion model and validated it against the experimental data of chlorophenol and dimethylphenol. Later, Fujioka *et al.* (2014b) have developed a one-dimensional model based on the irreversible thermodynamic model and used an iteration method to obtain the friction parameter.

To the best of author's knowledge, only Fujioka *et al.* (2014b) developed a distributed model for a spiral-wound RO process for wastewater treatment relying on the Spiegler and Kedem model. The model assumed zero pressure at the permeate side and was validated with experimental data of N-nitrosamine rejection.

Although there are number of methods applied for the removal of phenol from wastewater, spiral-wound RO process is selected in this research to investigate in detail the effectiveness of this process. Although experimental investigation would be desirable, it has been decided to resort to a model-based investigation methodology accepting the fact that a reliable model must be used for this purpose. Firstly, a detailed one-dimensional process model is developed relaxing the assumption made by Fujioka *et al.* (2014b). Secondly, several model parameters

have been estimated using a parameter estimation technique (Jarullah *et al.*, 2011) combined with experimental data of Srinivasan *et al.* (2010). Finally, the validated model is used in simulation mode to assess in detail the effect of various design and operating parameters on the performance of the RO process in terms of removal of phenol from wastewater.

2. Model Development

2.1. The assumptions

The following assumptions are considered to develop the new model:

a) A flat membrane sheet with negligible channel curvature.
b) Validity of the Spiegler-Kedem model for the transport of water and solute through the membrane.
c) Validity of the Darcy's law where a constant friction parameter is assumed to characterise the pressure drop.
d) Constant pressure of 1 atm on the permeate side.
e) Constant solute concentration in the permeated channel and the average value is calculated from the inlet and outlet calculated concentrations.
f) Complete mixing in the y-axis of the feed channel due to the existence of a network of spacers.
g) Isothermal process.

2.2 Governing Equations

The working equations of the non-linear solvent and molar solute fluxes are (Spiegler and Kedem, 1966):

$$J_{w(x)} = L_p \left(\Delta P_{b(x)} - \sigma \, \Delta \pi_{s(x)} \right)$$

(1)

$$J_{s(x)} = J_{w(x)} \, (1 - \sigma) \, \tilde{C}_{s(x)} + \omega \, \Delta \pi_{s(x)}$$

(2)

Where σ is the reflection coefficient and equals zero for complete coupling between the solvent and solute fluxes within the membrane and one if no coupling exists (The solution-diffusion model).

If σ =1, then Eq. (1) and (2) will be written as:

$$J_{w(x)} = L_p \left(\Delta P_{b(x)} - \Delta \pi_{s(x)} \right)$$

(3)

$$J_{s(x)} = B_s \left(C_{w(x)} - C_{p(av)}\right)$$

(4)

The trans-membrane pressure and the osmotic pressure are:

$$\Delta P_{b_{(x)}} = \left(P_{b(x)} - P_p\right)$$

(5)

$$\Delta\pi_{s(x)} = R\, T_b\, \left(C_{w(x)} - C_{p(av)}\right)$$

(6)

Since the solute flux is lower than volumetric solvent flux, the following equation work well:

$$J_{s(x)} = J_{w(x)}\, C_{p(av)}$$

(7)

While, the mean solute concentration is:

$$C_{s(x)}^{\sim} = \frac{C_{s(x)} - C_{p(av)}}{\ln\left(\frac{C_{s(x)}}{C_{p(av)}}\right)}$$

(8)

Substituting Eq. (6) in Eq. (2) and re-arrangement yields:

$$\Delta\pi_{s(x)} = \frac{J_{w(x)}\, C_{p(av)}}{\omega} - \frac{J_{w(x)}(1-\sigma)\, C_{s(x)}^{\sim}}{\omega}$$

(9)

Eq. (9) and Eq. (7) can be combined in Eq. (1) to form Eq. (10).

$$J_{w(x)} = L_p \left[\Delta P_{b_{(x)}} - \sigma \left(\frac{J_{w(x)}\, C_{p(av)}}{\omega} - \frac{J_{w(x)}\,(1-\sigma)\, C_{s(x)}^{\sim}}{\omega}\right)\right] \qquad (10)$$

Then, the expression of the solvent flux can be written as:

$$J_{w(x)} = \frac{L_p\, (\Delta P_{b_{(x)}})}{1 + \frac{\sigma\, C_{p(av)}\, L_p}{\omega} - \frac{C_{s(x)}^{\sim}(1-\sigma)\, L_p\, \sigma}{\omega}}$$

(11)

Based on Assumption d of constant pressure at the permeated side, Eq. (12) works well.

$$\frac{d\, \Delta P_{b(x)}}{dx} = \frac{d\, P_{b(x)}}{dx}$$

(12)

Relying the Assumption c, the friction parameter is used to characterise the feed pressure drop along the x-axis using Darcy's law.

$$\frac{dP_{b(x)}}{dx} = -b\, F_{b(x)}$$

(13)

While, the feed flow rate drop along the x-axis can be expressed as:

$$\frac{dF_{b(x)}}{dx} = -W\, J_{w(x)}$$

(14)

Dividing Eq. (12) and Eq. (14) yields:

$$\frac{d\,\Delta P_{b(x)}}{dF_{b(x)}} = \frac{b\,F_{b(x)}}{W\,J_{w(x)}}$$

(15)

Putting the value of solvent flux from Eq. (11) and re-arrangement with integration gives:

$$F^2_{b(x)} = F^2_{b(0)} + \left[\left(\Delta P^2_{b(x)} - \Delta P^2_{b(0)}\right)\left(\frac{W\,L_p}{b\,\emptyset_{(x)}}\right)\right]$$

(16)

Where $\emptyset_{(x)} = 1 + \frac{\sigma\, C_{p(av)}\, L_p}{\omega} - \frac{\tilde{C_{s(x)}}(1-\sigma)\,\sigma\, L_p}{\omega}$

(17)

Eq. (16) can be re-written as:

$$F_{b(x)} = F_{b(0)} + \left[\left(\Delta P^2_{b(x)} - \Delta P^2_{b(0)}\right)^{0.5}\left(\frac{W\,L_p}{b\,\emptyset_{(x)}}\right)^{0.5}\right]$$

(18)

Substituting Eq. (18) in Eq. (13) and take the integration will give an expression for the trans-membrane pressure.

$$\Delta P_{b(x)} = \Delta P_{b(0)} - b\,x\,F_{b(0)} - b\,x\,\Delta P_{b(x)}\left(\frac{W\,L_p}{b\,\emptyset_{(x)}}\right)^{0.5} + b\,x\,\Delta P_{b(0)}\left(\frac{W\,L_p}{b\,\emptyset_{(x)}}\right)^{0.5}$$

(19)

Combining Eq. (19) in Eq. (11), gives a correlation of solvent flux along the x-axis.

$$J_{w(x)} = \frac{L_p}{\emptyset_{(x)}}\left[\Delta P_{b(0)} - b\,x\,F_{b(0)} - b\,x\,\Delta P_{b(x)}\left(\frac{W\,L_p}{b\,\emptyset_{(x)}}\right)^{0.5} + b\,x\,\Delta P_{b(0)}\left(\frac{W\,L_p}{b\,\emptyset_{(x)}}\right)^{0.5}\right]$$

(20)

Another equation for feed flow rate can be derived by using Eq. (14) with integration.

$$F_{b(x)} = F_{b(0)} - \left[\left(\frac{W\,L_p}{\emptyset_{(x)}}\right)x\,\Delta P_{b(0)}\right] + \left[\left(\frac{W\,L_p}{\emptyset_{(x)}}\right)b\,F_{b(0)}\left(\frac{x^2}{2}\right)\right] + \left[\left(\frac{W\,L_p}{\emptyset_{(x)}}\right)^{1.5} b^{0.5}\Delta P_{b(x)}\left(\frac{x^2}{2}\right)\right] - \left[\left(\frac{W\,L_p}{\emptyset_{(x)}}\right)^{1.5} b^{0.5}\Delta P_{b(0)}\left(\frac{x^2}{2}\right)\right]$$

(21)

While, the feed pressure equation can be derived from using Eq. (13) with integration.

$$P_{b(x)} = P_{b(0)} - [b\,F_{b(0)}x] + \left[b\left(\frac{W\,L_p}{\emptyset_{(x)}}\right)\left(\frac{x^2}{2}\right)\Delta P_{b(0)}\right] - \left[b^2\left(\frac{W\,L_p}{\emptyset_{(x)}}\right)F_{b(0)}\left(\frac{x^3}{6}\right)\right] - \left[\left(\frac{W\,L_p}{\emptyset_{(x)}}\right)^{1.5} b^{1.5}\Delta P_{b(x)}\left(\frac{x^3}{6}\right)\right] + \left[\left(\frac{W\,L_p}{\emptyset_{(x)}}\right)^{1.5} b^{1.5}\Delta P_{b(0)}\left(\frac{x^3}{6}\right)\right]$$

(22)

Taking a total mass balance of the unit from $x = 0$ to any point along the x-axis, gives:

$$F_{b(0)} = F_{b(x)} + F_{p(x)}$$

(23)

The derivation of the above equation with the x-axis, gives:

$$\frac{dF_{b(x)}}{dx} = -\frac{dF_{p(x)}}{dx}$$

(24)

The volumetric permeated flow rate can be correlated in the form of Eq. (25):

$$F_{p(x)} = W\int_{x=0}^{x=x} J_{w(x)}\,dx$$

(25)

Also. substituting Eq. (20) in Eq. (25) and taking the integration, gives:

$$F_{p(x)} = F_{p(0)} + \left[\left(\frac{W\,L_p}{\emptyset_{(x)}}\right)x\,\Delta P_{b(0)}\right] - \left[\left(\frac{W\,L_p}{\emptyset_{(x)}}\right)b\,F_{b(0)}\left(\frac{x^2}{2}\right)\right] - \left[\left(\frac{W\,L_p}{\emptyset_{(x)}}\right)^{1.5} b^{0.5}\Delta P_{b(x)}\left(\frac{x^2}{2}\right)\right] + \left[\left(\frac{W\,L_p}{\emptyset_{(x)}}\right)^{1.5} b^{0.5}\Delta P_{b(0)}\left(\frac{x^2}{2}\right)\right]$$

(26)

The solute concentration increases along the x-axis, since the solute is retained by the membrane and can be calculated from Eq. (27) (Chen-Jen Lee, 2010).

$$\frac{d\frac{\left(C_{s(x)}\,F_{b(x)}\right)}{t_f\,W}}{dx} = -\frac{J_{w(x)}\,C_{p(av)}}{t_f} + \frac{J_{w(x)}\,C_{s(x)}}{t_f} + \frac{d}{dx}\left(D_{b(x)}\frac{dC_{s(x)}}{dx}\right)$$

(27)

The retained solute accumulates causes C_w to be greater than C_s in a thin laminar film on the high-pressure side of the membrane wall.

The solute concentration at the interface of the membrane can be included in this model by considering the theory of concentration polarisation.

$$\frac{\left(C_{w(x)} - C_{p(av)}\right)}{\left(C_{s(x)} - C_{p(av)}\right)} = \exp\left(\frac{J_{w(x)}}{k_{(x)}}\right)$$

(28)

Where, the mass transfer coefficient k is calculated using the following correlation of Wankat (1990):

$$k_{(x)} = 1.177 \left(\frac{F_{b(x)} D_{b(x)}^{\ 2}}{t_f^{\ 2} W L} \right)^{0.333} \quad (29)$$

Then, by substituting Eq. (28) and Eq. (7) in Eq. (4) with re-arrangement gives a correlation for average permeated concentration.

$$C_{p(av)} = \frac{B_s C_{s(x)} e^{\frac{J_{w(x)}}{k_{(x)}}}}{J_{w(x)} + B_s e^{\frac{J_{w(x)}}{k_{(x)}}}} \quad (30)$$

Following Assumption e, Eq. (30) will be used twice on the inlet and outlet dimensions to determine the exact average value of permeated solute concentration.

The rejection coefficient of the membrane and the total water recovery can be calculated from Eqs. (31) and (32) respectively (Srinivasan *et al.*, 2010).

$$Rej = \frac{C_{s(L)} - C_{p(av)}}{C_{s(L)}} \text{ x100} \quad (31)$$

$$Rec_{(Total)} = \frac{F_{p(Total)}}{F_{b(0)}} \text{ x100} \quad (32)$$

Where $F_{p(Total)}$ is the total permeated flow rate.

The proposed correlations of Koroneos (2007) to calculate the physical properties of seawater (density, viscosity and diffusion coefficient) are being considered identical to the analysis of dilute aqueous solutions of wastewater.

2.3 Parameter Estimation (determination of transport parameters)

Unknown parameters of the model and the operating conditions should be determined before solving the model equations. The aim of the optimisation is to accurately evaluate the values of these parameters depending on the experimental information that gives the best value of the performance criterion. Here, the gPROMS parameter estimation (Process System Enterprise Ltd., 2001) has been used to predict the model unknown parameters in a way that minimize the sum of square errors (SSE) between the experimental outlet concentration, average permeate concentration, outlet feed flow rate, total permeated water, outlet feed pressure and average solute rejection and the calculated values. This can be achieved by altering the model parameters from an initial guesstimate value to optimal values - usually referred to as the optimisation solver (Jarullah *et al.*, 2011). The gPROMS software provides a mathematical solver tool called as MXLKHD, which is based on maximum likelihood optimisation. The

optimisation problem is posed as a Non-Linear Programming (NLP) problem and is solved using a Successive Quadratic Programming (SQP) method.

The experiments of Srinivasan *et al.* (2010) have been done at different operating conditions of inlet feed pressure, concentration and temperature at fixed inlet feed flow rate. The developed model has five parameters, namely L_p, ω, B_s, σ and b.

The process model presented in Section 2 can be written in a compact form as follows:

$f(z, x(z), \dot{x}(z), u(z), v) = 0$; $[z_0, z_f]$

Where, z is the independent variable (length of membrane), $x(z)$ is the set of all differential and algebraic variables, $\dot{x}(z)$ represents the derivative of $x(z)$ with respect to length of membrane, $u(z)$ is the control variables and v denotes the constant parameters of the process. The membrane length under consideration $[z_0, z_f]$ and function f is assumed to be continuously differentiable with respect to all its arguments.

The parameter estimation problem can be formulated as follows:

Given: Time invariant parameters: Inlet feed concentration $C_{s(0)}$, flow rate $F_{b(0)}$, pressure $P_{b(0)}$ and temperature T_b

Measured variables data: Outlet measured concentration $C_{s(L)}$, average permeate concentration $C_{p(av)}$, outlet feed flow rate $F_{b(L)}$, outlet feed pressure $P_{b(L)}$, total permeated flow rate $F_{p(Total)}$ and average rejection $Rej_{(av)}$

Obtain: Water permeability coefficients L_p, solute permeability constants ω and B_s, reflection coefficient σ and friction parameter b

Minimising: The sum of square errors (SSE).

Subject to: Process model, Process constraints

For example, SSE for the outlet solute concentration is:

$$SSE = \sum_{i=1}^{N_{Data}} \left[C_{s,L}^{Exp.} - C_{s,L}^{Cal.} \right]^2 \quad (33)$$

In the above equation, N_{Data}, $C_{s(L)}^{Exp.}$ and $C_{s(L)}^{Cal.}$ are the numbers of test runs, experimental and calculated outlet feed concentration respectively.

The parameter estimation problem can be mathematically presented as follows:

The complete specification of a parameter estimation problem requires:

Min SSE

$L_p, \omega, B_s, \sigma, b$

Subject to: Equality constraints:

Process Model: $f(z, x(z), \dot{x}(z), u(z), v) = 0; \quad [z_0, z_f]$

Inequality constraints:

$$L_p^L \leq L_p \leq L_p^U$$

$$\omega^L \leq \omega \leq \omega^U$$

$$B_s^L \leq B_s \leq B_s^U$$

$$b^L \leq b \leq b^U$$

$$\sigma^L \leq \sigma \leq \sigma^U$$

The results of the parameter estimation showed that L_p varies between 1.56E-6 – 1.0E-6 m/atm s, ω varies between 0.1E-6 – 1.9E-6 kmol/m² s atm, B_s varies between 0.566E-6 – 1.9E-6 m/s, b varies between 12826 – 13537 atm s/m^4 and σ is 0.9 (dimensionless) for five different inlet feed concentrations. The total results and details of the parameter estimation approach can be found in Table 1. The description of experimental procedure and the operating conditions with the characteristics of the spiral-wound module (0.75 m² effective membrane area) can also be found in Srinivasan *et al.* (2010).

Table 1. The results of parameter estimation

No.	$C_{s(0)}x10^3$	$P_{b(0)}$	T_b	L_px10^6	$\omega x10^6$	B_sx10^6	b
1	2.125	4.93	32.5	1.56	0.145	1.850	13006
2	2.125	6.90	33.1	1.39	0.128	1.890	13042
3	2.125	8.90	33.0	1.39	0.100	1.900	13487
4	2.125	10.90	33.2	1.43	0.201	1.810	13537
5	2.125	14.80	34.0	1.26	0.295	1.130	12913
6	4.250	4.93	32.2	1.46	0.547	1.280	13008
7	4.250	6.90	32.8	1.34	0.228	1.380	13039
8	4.250	8.90	33.5	1.34	1.030	0.830	13487
9	4.250	10.90	33.9	1.27	0.355	0.566	13516
10	4.250	12.80	34.5	1.26	1.900	1.100	12867
11	4.250	14.80	34.5	1.27	1.330	1.170	12914
12	6.375	4.93	32.5	1.43	0.102	0.849	13005
13	6.375	6.90	33.0	1.16	1.900	0.934	13030
14	6.375	8.90	33.2	1.14	0.319	1.060	13461
15	6.375	10.90	33.5	1.04	0.245	0.877	13479
16	6.375	12.80	33.8	1.07	0.100	0.866	12839
17	6.375	14.80	34.0	1.15	1.050	0.627	12881
18	8.500	4.93	32.0	1.41	0.118	1.310	13003
19	8.500	6.90	32.5	1.22	0.277	1.400	13027
20	8.500	8.90	32.8	1.20	0.155	1.400	13465
21	8.500	10.90	33.0	1.22	1.370	1.230	13475
22	8.500	12.80	33.2	1.15	0.117	1.140	12844
23	8.500	14.80	33.5	1.19	0.562	1.120	12900
24	10.600	4.93	31.5	1.17	1.900	1.090	12985
25	10.600	6.90	32.2	1.11	1.900	1.170	13009
26	10.600	8.90	32.6	1.14	0.107	1.080	13480
27	10.600	10.90	32.8	1.13	0.110	1.080	13485
28	10.600	12.80	32.8	1.00	0.259	1.010	12826
29	10.600	14.80	33.0	1.09	1.820	0.854	12863
σ = 0.9							

3. Model validation

The simulation results of the proposed model are used to compare with the experimental data of Srinivasan *et al.* (2010) for the rejection of phenol from diluted aqueous solutions at feed flow rate of 3.333E-4 m^3/s.

Figs. 1 to 5 show the comparison of experimental and theoretical results of a phenol-water system for several operating conditions as follows:

Phenol rejection Rej, average phenol permeate concentration $C_{p(av)}$, outlet phenol concentration $C_{s(L)}$, outlet feed pressure $P_{b(L)}$ and outlet feed flow rate $F_{b(L)}$.

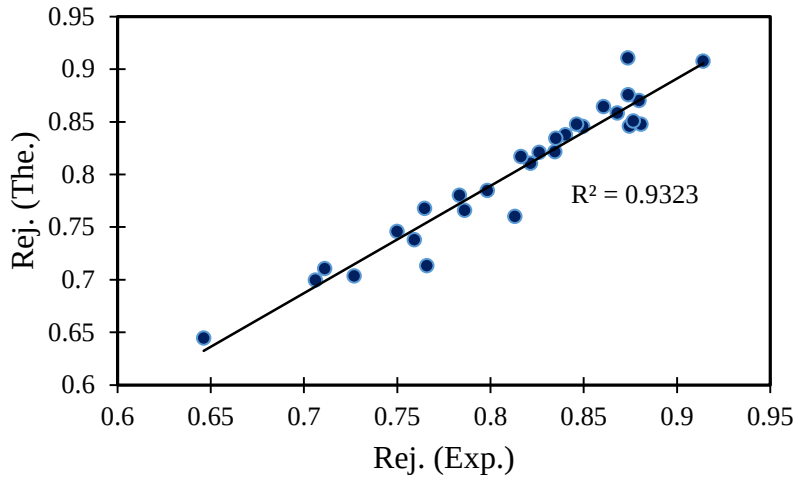

Fig. 1. Comparison of theoretical and experimental results of phenol rejection

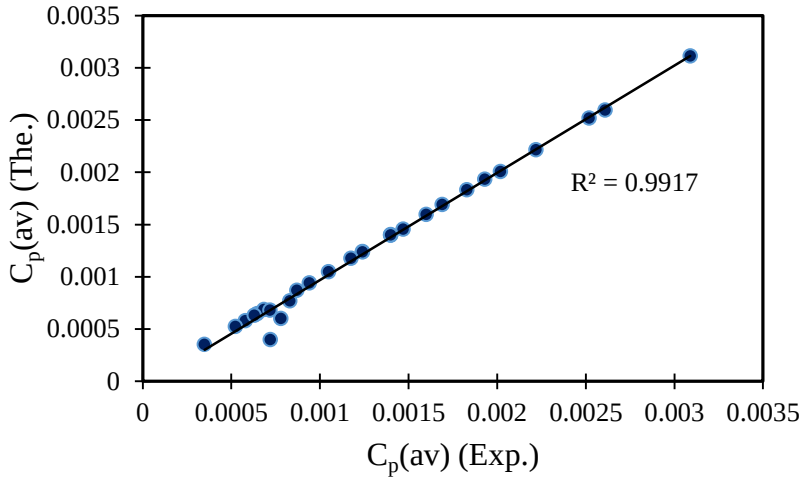

Fig. 2. Comparison of theoretical and experimental results of the average permeate concentration

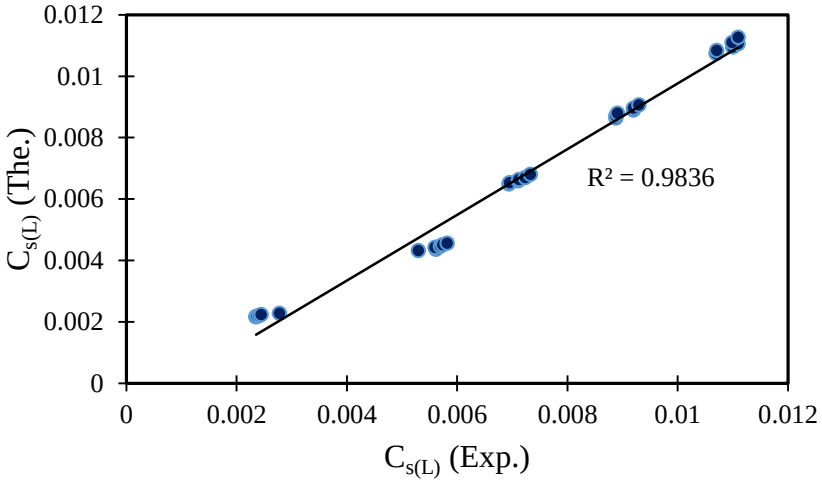

Fig. 3. Comparison of theoretical and experimental results of the outlet phenol concentration

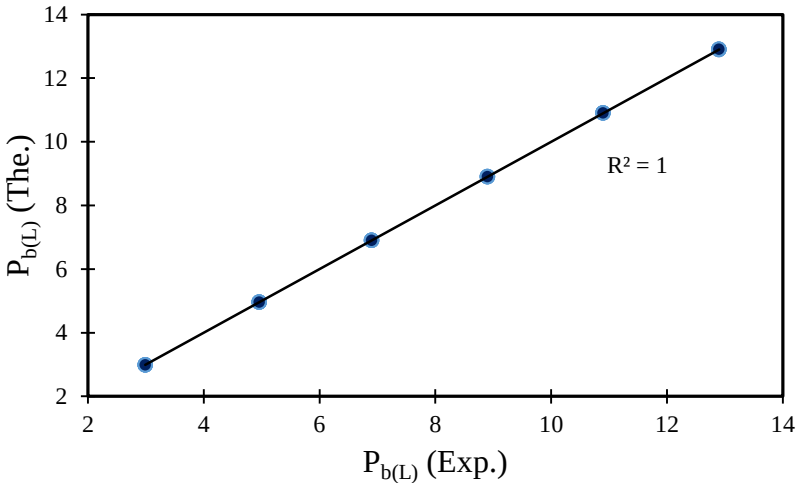

Fig. 4. Comparison of theoretical and experimental results of the outlet feed pressure

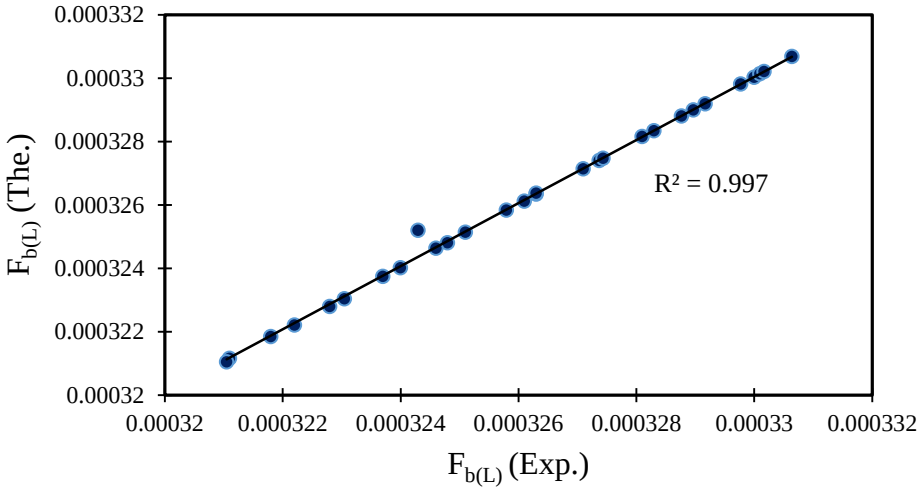

Fig. 5. Comparison of theoretical and experimental results of the outlet feed flow rate

Generally, the predicted values of the theoretical model are in a good agreement with experimental ones over the ranges of pressure and concentration with linear correlations of R^2 = 0.932, 0.991, 0.983, 1.0 and 0.997 respectively.

4. Simulation results of the membrane separation process

The effect of operating parameters such as the solute concentration, applied pressure and feed flow rate are important to determine the optimum conditions for the competent separation of contaminated water.

Here, the model validated in Section 3 is used to investigate the effect of several operational conditions on the performance of the process.

The experimental values and model predictions of the total permeated flow rate ($F_{p(L)}$) of phenol solutions versus the operating inlet feed pressure for two different inlet feed concentrations is presented in Fig. 6.

The permeated flow rate remains linear versus the applied pressure. Also, it increases due to an increase in the operating pressure. Eq. (1) confirms that the trans-membrane pressure can be considered as the driving force of RO process. Therefore, the recovery rate will increase due to an increase in feed pressure. Fig. 6 also shows the reduction of permeated flow rate due to an increase in inlet feed concentration. This is attributed to an increase in the osmotic pressure occurring due to an increase in the concentration polarisation. Furthermore, a good agreement between the model prediction and experimental data was observed for the parameters tested.

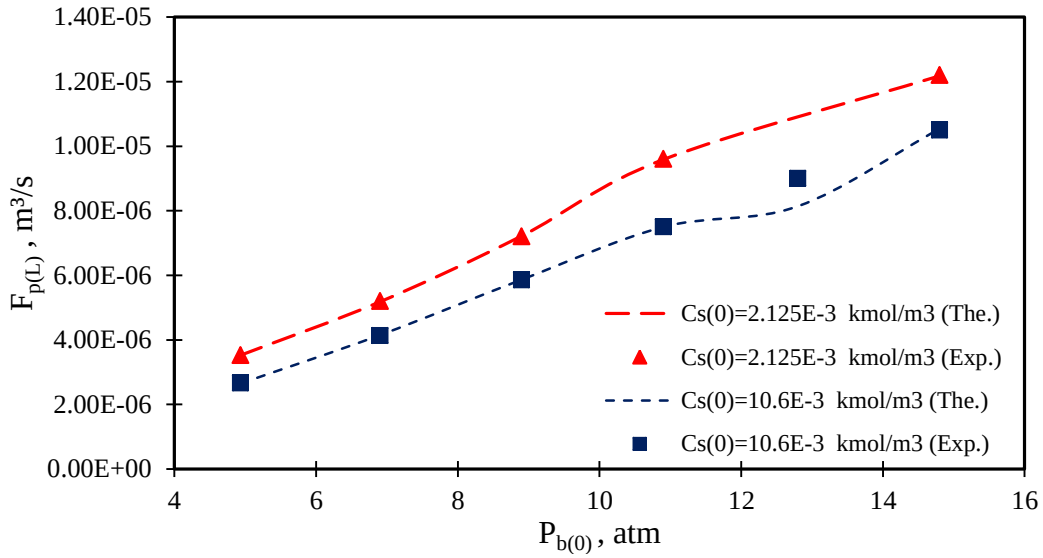

Fig. 6. Experimental and model prediction of total permeated flow rate versus inlet feed pressure for two different inlet feed concentrations at ($F_{b(0)}$ = 3.333E-4 m³/s)

Generally, the impact of increasing operating pressure can be recognised in two different behaviours against the solute rejection. Firstly, the water flux increases due to an increase in the trans-membrane pressure, which causes a lower permeate concentration and a higher solute rejection. Secondly, the increasing operating pressure results in an increase of the solute accumulation over the wall membrane, which causes higher concentration polarisation and a lower solute rejection. Therefore, different behaviours of solute rejection, depending on the membrane type and the operating parameters, are expected.

Fig. 7 shows the impact of increasing the inlet pressure on phenol rejection for feed solutions of two different concentrations. Fig. 7 provides a comparison of the model prediction and the

experimental values and clearly confirms the consistency of the model developed. However, the model overestimated the case of low feed concentration and this can be attributed to lower accuracy of parameter estimation at very low phenol concentration.

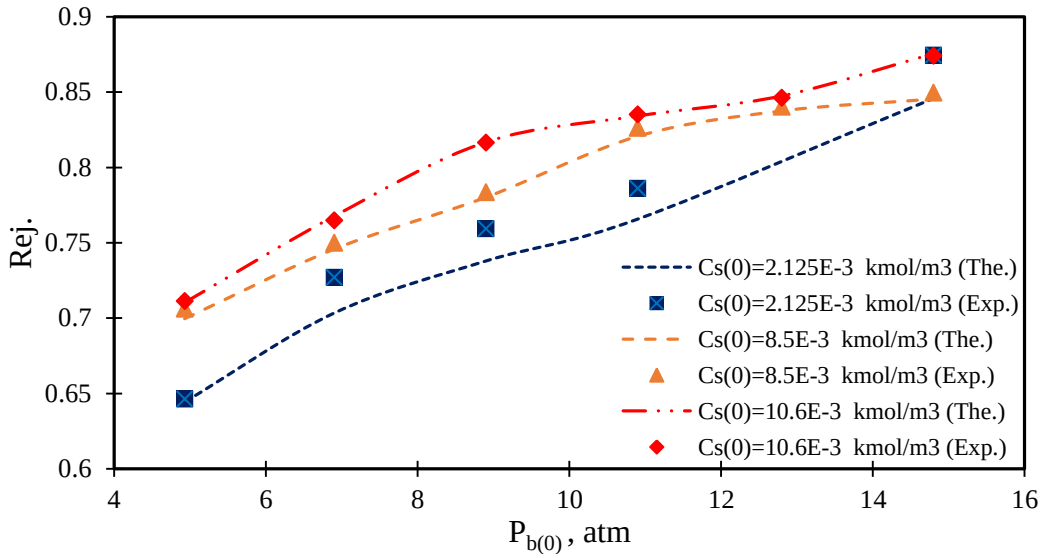

Fig. 7. Experimental and model prediction of phenol rejection versus inlet feed pressure of different inlet feed concentrations at ($F_{b(0)}$ = 3.33E-4 m^3/s)

It is observed that the solute rejection increases over the whole applied pressure for the three inlet feed concentrations. This is due to the fact that the water flux is more affected by pressure than solute flux as can be verified in Eqs. (1) and (2).

In addition, high inlet feed concentration yields an increase of the solute rejection and this may be due to several reasons. Firstly, it seems that the membrane solute isolation intensity increases due to an increase in the applied concentration (Al-Obaidi and Mujtaba, 2016). It is interesting to note that despite increasing the permeate concentration by increasing the inlet feed concentration, this increase is lower (not comparable) than the increase of feed concentration along the membrane length. Therefore, the solute rejection will increase according to Eq. (32) due to a higher increase in the feed concentration. A similar trend was observed for all the three types of tested membranes used by Gómez *et al.* (2009).

The prediction of the developed model is compared with the experimental findings of phenol rejection at low and high inlet feed concentration of Srinivasan *et al.* (2010) and with both the developed models of Srinivasan *et al.* (2010) and Sundaramoorthy *et al.* (2011a) predictions as can be shown in Table 2 (Note: Parameter estimation results shown in Table 1 have been used for Sundaramoorthy *et al.* (2011a) calculations). Table 2 confirms that the findings of the

new developed model are quite close to experimental results and compare well with other earlier models.

Table 2. Comparison of the experimental phenol rejection with the prediction of the developed model and Srinivasan *et al.* (2010) and Sundaramoorthy *et al.* (2011a) models at inlet feed flow rate ($F_{b(0)}$= 3.33E-4 m³/s)

No.	$P_{b(0)}$, atm	T_b, °C	$C_{s(0)}$ $E3$ kmol/m³	Rej. Exp.	Rej. Model	Rej. Srinivasan *et al.* (2010)	Rej. Sundaramoorthy *et al.* (2011a)
1	4.93	32.5	2.125	0.646	0.644	0.642	0.634
2	6.90	33.1	2.125	0.727	0.703	0.698	0.698
3	8.90	33.0	2.125	0.759	0.737	0.733	0.733
4	10.90	33.2	2.125	0.786	0.765	0.758	0.761
5	14.80	34.0	2.125	0.874	0.845	0.790	0.843
6	4.93	32.2	4.250	0.766	0.713	0.680	0.700
7	6.90	32.8	4.250	0.813	0.759	0.737	0.753
8	8.90	33.5	4.250	0.861	0.864	0.772	0.859
9	10.90	33.9	4.250	0.873	0.910	0.796	0.908
10	12.80	34.5	4.250	0.880	0.847	0.813	0.844
11	14.80	34.5	4.250	0.876	0.850	0.813	0.839
12	4.93	32.5	6.375	0.798	0.784	0.696	0.772
13	6.90	33.0	6.375	0.821	0.810	0.754	0.803
14	8.90	33.2	6.375	0.834	0.821	0.790	0.816
15	10.90	33.5	6.375	0.868	0.858	0.814	0.855
16	12.80	33.8	6.375	0.879	0.870	0.830	0.867
17	14.80	34.0	6.375	0.914	0.907	0.844	0.905
18	4.93	32.0	8.500	0.706	0.699	0.704	0.684
19	6.90	32.5	8.500	0.750	0.745	0.764	0.737
20	8.90	32.8	8.500	0.783	0.780	0.800	0.774
21	10.90	33.0	8.500	0.826	0.820	0.824	0.816
22	12.80	33.2	8.500	0.840	0.837	0.840	0.834
23	14.80	33.5	8.500	0.849	0.845	0.854	0.842
24	4.93	31.5	10.600	0.711	0.710	0.708	0.689
25	6.90	32.2	10.600	0.764	0.767	0.770	0.757
26	8.90	32.6	10.600	0.816	0.816	0.806	0.811
27	10.90	32.8	10.600	0.835	0.834	0.830	0.829
28	12.80	32.8	10.600	0.846	0.847	0.847	0.843
29	14.80	33.0	10.600	0.874	0.875	0.861	0.872

Fig. 9 depicts an increase in the average permeate concentration of phenol and a decrease in the total permeate flow rate by increasing the applied feed concentration. This is because the water flux and total permeate flow rate are retarded along the membrane length by increasing the applied concentration due to the increase in the osmotic pressure, which reduces the

driving force of water flux. The permeate concentration of phenol will increase as a result of this. For this same reason, it is expected that increasing the inlet feed concentration will cause an increase in the outlet phenol concentration in addition to increasing the retentate flow rate as can be shown in Fig. 10.

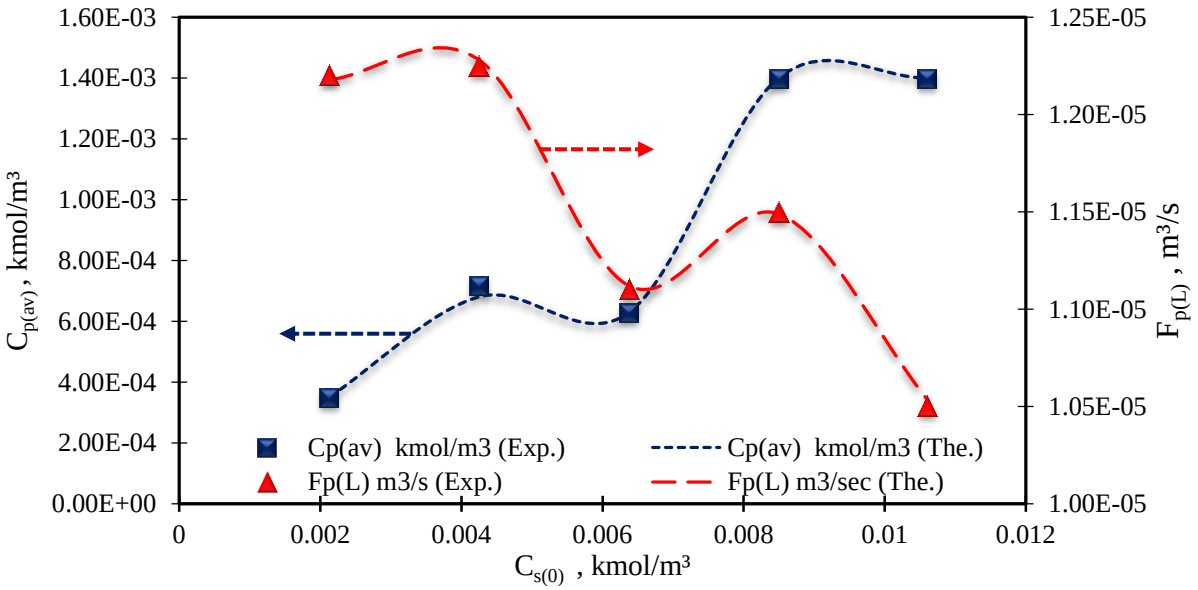

Fig. 9. Experimental and model predictions of phenol permeated concentration and outlet permeated flow rate versus inlet feed concentration, (inlet feed conditions, 14.8 atm and 3.33E-4 m³/s)

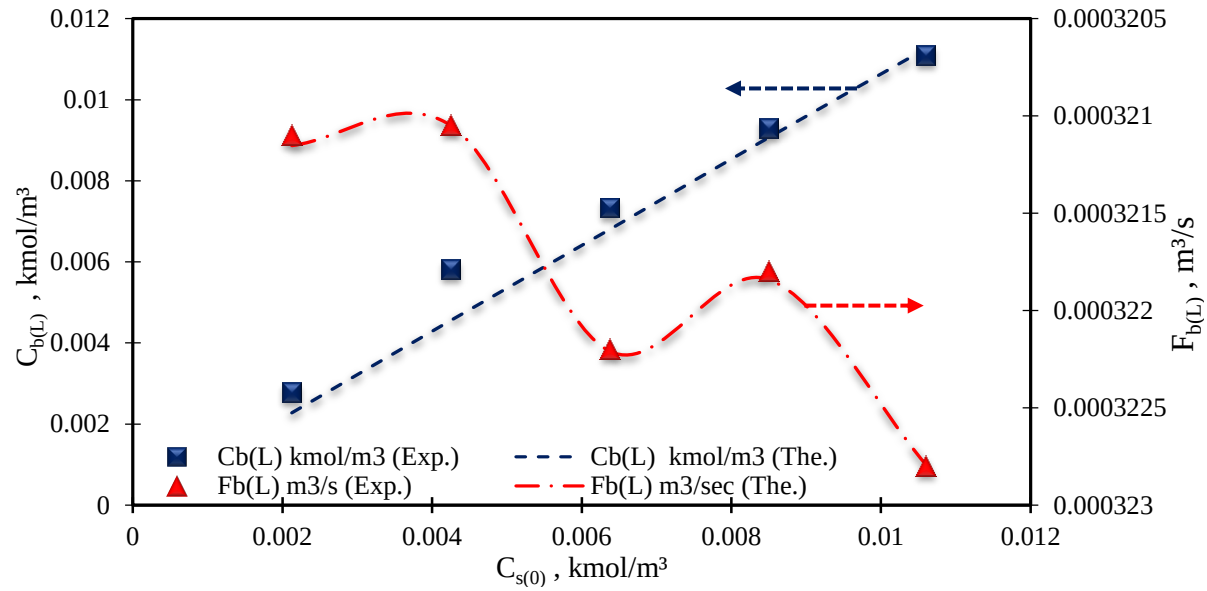

Fig. 10. Experimental and model predictions of retentate phenol concentration and retentate flow rate versus inlet feed concentration, (inlet feed conditions, 14.8 atm and 3.33E-4 m³/s)

More often than not, an increment in feed flow rate causes a slight increase in phenol rejection for all the tested feed concentrations as can be shown in Figs. 11 and 12. It appears that there is a miscorrelation between these two competitive impacts, which determine the solute rejection as a result to increase in the inlet flow rate. The first one leads to an increase in the friction along the membrane, which reduces the water flux and solute rejection. While, the second one leads to an increase in the turbulence that causes a reduction in the concentration polarisation and wall membrane concentration, which increases water flux and solute rejection. It seems that the second impact is slightly more predominant in the process, which possibly causes a slight increase in phenol rejection.

To justify the above findings further, Figs. 11 and 12 show two different responses of solute rejection versus inlet feed concentration given the applied pressure.

Firstly, at high operating pressure conditions of 14.8 atm, it seems that the solute rejection decreases by increasing inlet feed concentration up to 4.25E-3 kmol/m³ (Fig. 11). However, increasing the applied concentration to 8.5E-3 and 10.6E-3 kmol/m³ causes an increase in the solute rejection (Fig. 11). The reason behind the first response is that an increment in feed concentration causes an increase in the osmotic pressure, which reduces the driving force of water flux and therefore reduces the solute rejection. While, using a higher inlet feed concentration at high applied pressure conditions leads to an increase in the solute rejection. This is due to an increase in the membrane isolation intensity at these conditions. However, it seems that inlet feed concentration of 6.375E-3 kmol/m³ has a similar high solute rejection (Figs. 11 and 12) and this may yield the optimum condition of feed concentration to perform higher solute rejection.

Secondly, at low operating pressure conditions of 8.9 atm, it seems that the feed concentration has the same role in controlling the solute rejection except for the case of 6.375E-3 kmol/m³ feed concentration. The impact of increasing inlet feed concentration will lead to an increase in the solute rejection whatever inlet feed flow rate is used. Srinivasan *et al.* (2011) and Sundaramoorthy *et al.* (2011b) confirmed the same findings for dimethylphenol and chlorophenol respectively. Also, the impact of inlet feed flow rate at higher feed pressure is clearly noticeable than the lower feed pressure as can be seen in Figs. 11 and 12. This is caused by the contribution of feed pressure in lifting the solute rejection.

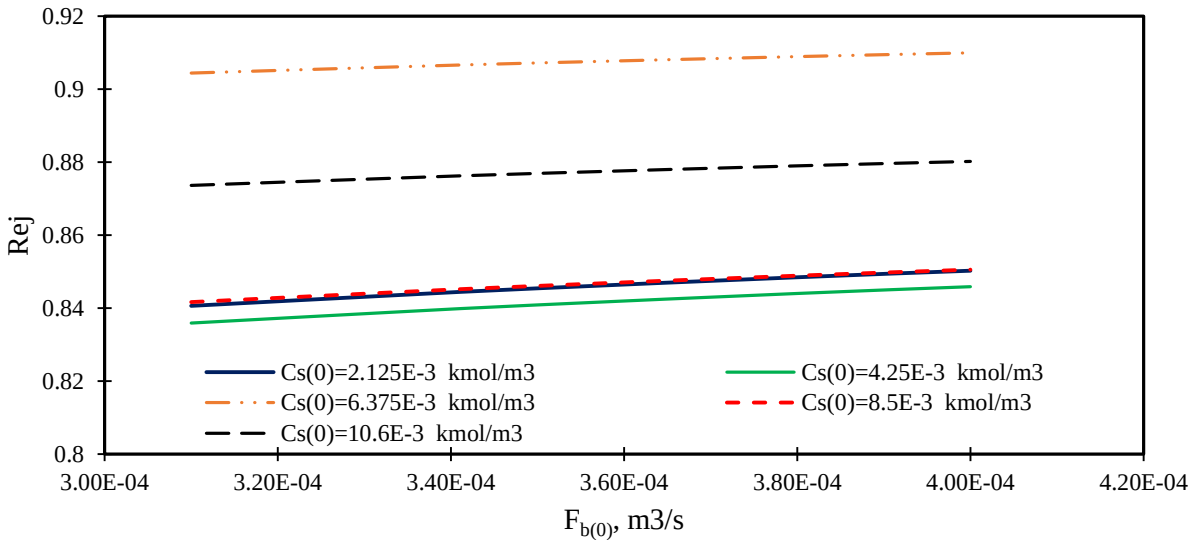

Fig. 11. Phenol rejection versus inlet feed flow rate for different inlet feed concentration (inlet feed conditions, 14.8 atm and 33 °C)

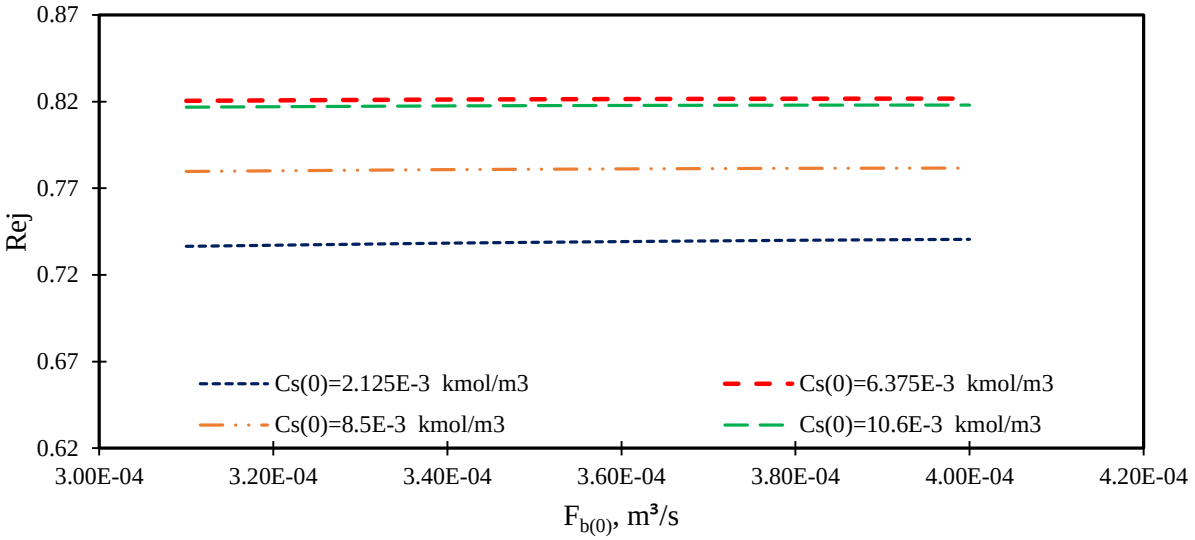

Fig. 12. Phenol rejection versus inlet feed flow rate for different inlet feed concentration (inlet feed conditions, 8.9 atm and 33 °C)

The above results readily show the feasibility of acceptable mitigation of phenol concentration found in industrial wastes using an individual RO module of 0.75 m² membrane effective area, which confirms the potential of RO as a competitive technique for wastewater treatment. Having said this, the model can be advanced to consider the performance of the RO process at higher feed concentrations after embedding the fouling impact on the transport parameters of the membrane.

5. Conclusions

Reverse Osmosis is a key treatment process in water reclamation applications for the removal of organic matter, inorganic chemicals. It is therefore essential to generate an accurate model with a reliable process design, which can describe the process behaviour and more accurately. The research conducted in this study serves this precise purpose and explores the spiral-wound RO process as an alternative approach for concentration reduction of impurities in industrial wastewater. The investigated pollutant was phenols which are considered as extremely toxic compounds with several harmful effects for humans, the environment and the aquatic life. Taking into account one-dimensional character of the process (x-axis as the spatial dimension in the direction of the feed flow), an efficient steady state model applicable for dilute binary aqueous solution in a spiral-wound RO process has been developed based on the theory of the Spiegler and Kedem model. The model can predict a variety of operating parameters at each point along the two sides of the membrane length. The model algorithm has been resolved using the gPROMS software by assuming constant temperature and permeate pressure. The gPROMS parameter estimation tool was used to predict the model unknown parameters (water and solute permeability constants, reflection coefficient and friction parameter). The predictions of this model in respect of the operating conditions compare favourably to phenol rejection experimental data results available in the literature, and show a good agreement with an accepted convergence for most operating parameters. Finally, the impact of several operational conditions on the performance of the process has been studied, which show that there is an optimum condition of feed concentration to perform higher solute rejection. This research can readily be used as a basis for a complete model for spiral-wound RO membranes used in wastewater treatment.

Nomenclature

b : Feed channel friction parameter (atm s/m^4).

B_s : Solute transport coefficient considering the Solution-diffusion model (Eq. 4) (m/s).

$C_{p(av)}$: Average permeate solute concentration in the permeate channel (kmol/m^3).

$C_{s(x)}$: Brine solute concentration in each point along the x-axis (kmol/m^3).

$\tilde{C}_{s(x)}$: The mean solute concentration in each point along the x-axis (kmol/m^3).

$C_{w(x)}$: Solute concentration at the membrane wall in each point along the x-axis (kmol/m^3).

$D_{b(x)}$: Diffusivity of feed in each point along the x-axis (m^2/s).

$F_{b(x)}$: Feed flow rate in each point along the x-axis (m^3/s).

$F_{p(x)}$: Permeate flow rate in each point along the x-axis (m^3/s).

$F_{p(Total)}$: Total permeated flow rate for the whole unit (m^3/s).

$J_{s(x)}$: Solute molar flux through the membrane in each point along the x-axis ($kmol/m^2\ s$).

$J_{w(x)}$: Water flux in each point along the x-axis (m/s).

$k_{(x)}$: Mass transfer coefficient in each point along the x-axis (m/s).

L : Length of the membrane (m).

L_p : Solvent transport coefficient (m/atm s).

$P_{b(x)}$: Feed pressure in each point along the x-axis (atm).

P_p : Permeate pressure (atm).

R : Gas low constant $\left(R = 0.082 \frac{atm\ m^3}{K\ kmol}\right)$.

$Rec_{(Total)}$: Total water recovery for the whole unit (dimensionless).

Rej : The rejection coefficient of the membrane (dimensionless).

T_b : Feed temperature (°C).

t_f : Feed spacer thickness (m).

W : Width of the membrane (m).

x : The dimension along the x-axis (m).

Δx : Length of sub-section (m).

$\Delta P_{b(x)}$: Trans-membrane pressure in each point along the x-axis (atm).

$\Delta\pi_{s(x)}$: The osmotic pressure difference in each point along the x-axis (atm).

σ : Reflection coefficient (dimensionless).

ω : The solute permeability constant of the membrane (Spiegler-Kedem model) ($kmol/m^2\ s\ atm$).

$\emptyset_{(x)}$: Parameter defined in Eq. (17).

References

Ahmad A. L., Chong M. F. and Bhatia S. 2007. Mathematical modeling of multiple solutes system for reverse osmosis process in palm oil mill effluent (POME) treatment. *Chemical Engineering Journal*, 132, 183-193.

Al-Obaidi M. A. and Mujtaba I. M. 2016. Steady state and dynamic modeling of spiral wound wastewaterreverse osmosis process. *Computers and Chemical Engineering*, 90, 278-299.

Alzahrani S., Mohammad A.W., Hilal N., Abdullah P. and Jaafar O., 2013. Comparative study of NF and RO membranes in the treatment of produced water—Part I: Assessing water quality. *Desalination*, 315, 18-26.

Bódalo-Santoyo A., Gómez-Carrasco J. L., Gómez-Gómez E., Máximo-Martin M. F. and Hidalgo-Montesinos A. M. 2004. Spiral-wound membrane reverse osmosis and the treatment of industrial effluents. *Desalination*, 160, 15l-l58.

Lee C-J , Chen Y-S and Wang G. B. 2010. A dynamic simulation model of reverse osmosis desalination systems. The 5th International Symposium on Design, Operation and Control of Chemical Processes, PSE ASIA, Singapore.

Elhalwagi, M. M. 1992. Synthesis of reverse-osmosis networks for waste reduction, *AICHE Journal, 38*, 1185-1198.

Fritzmann C., Löwenberg J., Wintgens T. and Melin T. 2007. State-of-the-art of reverse osmosis desalination. *Desalination,* 216, 1-76.

Fujioka T. 2014a. *Assessment and optimisation of N-nitrosamine rejection by reverse osmosis for planned potable water recycling applications*. Ph.d Theses, University of Wollongong.

Fujioka T., Khan S. J., Mcdonald J. A., Roux A., Poussade Y., Drewes J. E. and Nghiem L. D. 2014b. Modelling the rejection of N-nitrosamines by a spiral-wound reverse osmosis system: Mathematical model development and validation. *Journal of Membrane Science, 454,* 212-219.

Gami A. A., Shukor M. Y., Abdul Khalil K., Dahalan F. A., Khalid A. and Ahmad S. A., 2014. Phenol and its toxicity. *Journal of Environmental Microbiology and Toxicology*, 2(1), 11-24.

Geraldes V., Escórcio Pereira N. and Norberta de Pinho M. 2005. Simulation and optimization of medium-sized seawater reverse osmosis processes with spiral-wound modules. *Industrial & Engineering Chemistry Research,* 44(6), 1897-1905.

Goh P. S., Matsuura T., Ismail A. F. and Hilal N., 2016. Recent trends in membranes and membrane processes for desalination. *Desalination*, 391, 43-60.

Gómez J., León G., Hidalgo A., Gómez M., Murcia M. and Griñán G. 2009. Application of reverse osmosis to remove aniline from wastewater. *Desalination,* 245, 687-693.

Jarullah A. T., Mujtaba I. M. and Wood A. S. 2011. Kinetic parameter estimation and simulation of trickle-bed reactor for hydrodesulfurization of crude oil. *Chemical Engineering Science,* 66, 859-871.

Kaghazchi T., Mehri M., Takht Ravanchi M. and Kargari A. 2010. A mathematical modeling of two industrial seawater desalination plants in the persian gulf region. *Desalination, 252,* 135-142.

Koroneos C., Dompros A. and Roumbas G. 2007. Renewable energy driven desalination systems modelling. *Journal of Cleaner Production, 15,* 449-464.

Lee, S. and Lueptow R. M. 2001. Rotating reverse osmosis: a dynamic model for flux and rejection. *Journal of Membrane Science,* 192, 129-143.

Mangrulkar P. A., Bansiwal A. K. and Rayalu, S. S. 2008. Adsorption of phenol ando chlorophenol on surface altered fly ash based molecular sieves. *Chemical Engineering Journal,*138, 73-77.

Mohammed A. E., Jarullaha A. T., Gheni S. A. and Mujtaba I. M. 2016. Optimal design and operation of an industrial three phase reactor for the oxidation of phenol. *Computers and Chemical Engineering,* 94, 257-271.

Mujtaba I. M. 2012. The Role of PSE Community in Meeting Sustainable Freshwater Demand of Tomorrow's World via Desalination., In Computer Aided Chemical Engineering- 31, I.A. Karimi and Rajagopalan Srinivasan (Editors), Vol 31, 91-98, Elsevier.

Murthy Z. V. P. and Gupta S. K. 1999. Sodium cyanide separation and parameter estimation for reverse osmosis thin film composite polyamide membrane. *Journal of Membrane Science, 154,* 89-103.

Oh H., Hwang T. and Lee S. 2009. A simplified model of RO systems for seawater desalination. *Desalination,* 238, 128-139.

Process System Enterprise Ltd. 2001. *gPROMS Introductory User Guide.* London: Process System Enterprise Ltd.

Sagne C., Fargues C., Broyart B., Lameloise M. and Decloux M. 2005. Modeling permeation of volatile organic molecules through reverse osmosis spiral-wound membranes. *Journal of Membrane Science,* 330, (1-2), 40-50.

Schutte C. F. 2003. The rejection of specific organic compounds by reverse osmosis membranes. *Desalination,* I58, 285-294.

Senthilmurugan S., Ahluwalia A. and Gupta S. K. 2005. Modeling of a spiral-wound module and estimation of model parameters using numerical techniques. *Desalination,* 173, 269-286.

Soltanieh M. and Gill W. 1981. Review of reverse osmosis membranes and transport models. *Chemical Engineering Communications,* 12, 279-363.

Spiegler K. S. and Kedem O. 1966. Thermodynamics of hyperfiltration (reverse osmosis): criteria for efficient membranes. *Desalination,* 1**,** 311-326.

Srinivasan G., Sundaramoorthy S. and Murthy D.V.R. 2010. Spiral wound reverse osmosis membranes for the recovery of phenol compounds-experimental and parameter estimation studies. *American Journal of Engineering and Applied Science,* 3(1), 31-36.

Srinivasan G., Sundaramoorthy S. and Murthy D.V.R. 2011. Validation of an analytical model for spiral wound reverse osmosis membrane module using experimental data on the removal of dimethylphenol. *Desalination,* 281, 199-208.

Sundaramoorthy S., Srinivasan G. and Murthy D. V. R. 2011a. An analytical model for spiral wound reverse osmosis membrane modules: Part I — Model development and parameter estimation. *Desalination, 280(1-3),* 403-411.

Sundaramoorthy S., Srinivasan G. and Murthy D. V. R. 2011b. An analytical model for spiral wound reverse osmosis membrane modules: Part II — Experimental validation. *Desalination,* 277(1-3), 257-264.

Traves W.H., Gardner E.A., Dennien B. and Spiller D. 2008. Towards indirect potable reuse in south east Queensland. *Water Science Technolgy*, 58, 153-161.

Verliefde A., Cornelissen E., Heijman S., Verberk J., Amy G., Van der Bruggen B. and Dijk J. 2009. Construction and validation of a full-scale model for rejection of organic micropollutants by NF membranes. *Journal of Membrane Science,* 339, 10-20.

Wang K., Abdalla A. A., Khaleel M. A., Hilal N. and Khraisheh M. K., 2016. Mechanical properties of water desalination and wastewater treatment membranes. Accepted in Desalination, http://dx.doi.org/10.1016/j.desal.2016.06.032

Wankat P. C. 1990. Rate-Controlled Separation. Ist Edn. , Springer, ISBN: 10: 1851665218, pp: 873.